Methanotroph phenotypic heterogeneity in a methane-oxygen counter gradient

Delaney G. Beals and Aaron W. Puri[#]

Department of Chemistry and the Henry Eyring Center for Cell and Genome Science, University of Utah, Salt Lake City, Utah, USA

Keywords: methanotroph, methane, model ecosystem, phenotypic heterogeneity

#Corresponding author:
Aaron W. Puri
315 S 1400 E Rm 2020
Salt Lake City, UT 84112
USA
(801) 213-1408
a.puri@utah.edu

ABSTRACT

Connecting genes to phenotypic traits in bacteria is often challenging because of a lack of environmental context in laboratory settings. Laboratory-based model ecosystems offer a means to better account for environmental conditions compared to standard planktonic cultures, and can help link genotypes and phenotypes. Here, we present a simple, cost-effective, laboratory-based model ecosystem to study aerobic methane-oxidizing bacteria (methanotrophs) within the methane-oxygen counter gradient typically found in the natural environment of these organisms. Culturing the methanotroph *Methylomonas* sp. strain LW13 in this system resulted in formation of a distinct horizontal band at the intersection of the counter gradient, which we discovered was not due to increased numbers of viable bacteria at this location but instead to an increased amount of polysaccharides. We also discovered that different methanotrophic taxa form polysaccharide bands with distinct locations and morphologies when grown in the methane-oxygen counter gradient. By comparing transcriptomic data from LW13 growing within and surrounding this band, we identified genes correlated with polysaccharide band formation within the model ecosystem and validated the involvement of these genes with knockout strains. Notably, these genes were also required for cell growth in the system. This work highlights the use of a laboratory-based model ecosystem that more closely mimics the natural environment to uncover methanotroph phenotypes missing from standard planktonic cultures, and to link these phenotypes with their genetic determinants.

INTRODUCTION

Despite the explosion in availability of bacterial genomic data, linking genes with organismal phenotypes remains difficult. One reason is that assigning gene functions can be hindered by a lack of ecological context in the lab, as bacteria are removed from the environments where they evolved. Laboratory-based model ecosystems are a powerful tool that can be used to more closely recapitulate the natural environment than simple planktonic cultures [1, 2].

Aerobic methane-oxidizing bacteria (methanotrophs) play important roles in biogeochemical cycling, bioremediation, and sequestration of the potent greenhouse gas methane [3–5]. These bacteria require methane as a carbon and energy source, and oxygen as an electron acceptor and atom donor the methane monooxygenase reaction. In the environment, methanotrophs often exist in opposing gradients of oxygen and methane, where oxygen diffuses from the atmosphere or water column above, and methane diffuses up from anaerobic decomposition processes below [6–9]. Studies using methane enrichments of sediment have consistently observed dynamic population flux amongst methanotrophs in response to shifting oxygen and methane availability [10, 11]. Methanotrophs are therefore particularly shaped by the spatial heterogeneity of their environment, however in the laboratory these organisms have primarily been studied using homogenous planktonic cultures. This is likely impeding our ability to both understand the molecular details of methanotroph physiology, and to optimize these details for industrial processes and climate change mitigation [12, 13].

Culturing methanotrophs within a spatially resolved model ecosystem may help uncover phenotypes that are otherwise undetectable in planktonic cultures. Previously, researchers demonstrated that growing methanotrophs within opposing gradients of methane and oxygen in the lab is feasible using a variety of methods. In some examples, soil was suspended on a PTFE membrane that allowed gas exchange from the methane supply below [6, 14, 15]. In other cases, sediment was added to semi-solid agarose and exposed to opposing chambers of air and methane [16, 17]. To our knowledge, these systems have been primarily used to isolate and classify methanotrophs from mixed methane-oxidizing consortia and have not yet been used to collect molecular-level information about the physiology of methanotrophs under opposing methane and oxygen gradients.

Inspired by the methane-taxis assay used by Dedysh and coworkers [18], we created a simple, inexpensive, laboratory-based model ecosystem using a disposable syringe that enables researchers to culture methanotrophs in a spatially resolved context. We first characterized the counter gradients of methane and oxygen in this model ecosystem, referred to as the gradient syringe, and then cultured individual methanotrophs within the system. Using this method, we observed a horizontal band form at the intersection of the counter gradient even though the entire system was uniformly inoculated with bacterial cells. We discovered that this band was due to an increased amount of polysaccharides at this depth, but not an increased amount of viable cells. Through transcriptional analysis across layers of the gradient syringe, we identified many genes with differential expression in *Methylomonas* sp. strain LW13 (LW13) growing at different depths of the system. We subsequently confirmed using genetics that three of these genes are important for production of the polysaccharide band, and that these genes are also required for growth in the gradient syringe but not in planktonic culture. These results provide insights into the heterogenous physiological responses of methanotrophs growing under the opposing methane and oxygen gradients they encounter in the environment and highlight the potential of this laboratory-based model ecosystem to uncover the genes responsible for these phenotypes.

RESULTS

Different methanotrophic taxa form horizontal bands with distinct locations and morphologies when grown in the gradient syringe model ecosystem

We established a simple laboratory-based model ecosystem to cultivate methanotrophs using semi-solid agarose in disposable syringes (**Fig 1A**). Syringes were equipped with a sterile filter tip and filled with agarose, bacterial inoculum, and nitrate mineral salt medium. We inoculated gradient syringes with individual cultures of four methanotrophs isolated from Lake Washington, Seattle, USA [19]. All methanotrophs inoculated into the gradient syringe formed a horizontal band around the midpoint of the

agarose plug in as few as three days, even though the agarose was uniformly inoculated with bacteria, as observed previously in more complex setups [16, 17]. With additional days of incubation and replenishment of methane in the syringe headspace, this band became more pronounced and opaque.

Different strains of methanotrophs reproducibly formed the band at different rates and depths when they were individually cultured in the gradient syringe (**Fig 1B**). The gammaproteobacterium LW13 formed a 2.1 ± 0.04 mm thick band within three days of incubation at a depth range within 25-30 mm from the oxygen side of the syringe. *Methylobacter tundripaludum* 21/22 formed a 0.12 ± 0.05 mm thick band within four days of incubation at a depth range of 18-24 mm within the gradient syringe. When two methanotrophic alphaproteobacteria were individually cultured in the gradient syringe, they formed bands that were less opaque and more diffuse than the gammaproteobacteria. *Methylosinus* sp. LW3 formed a 0.4 ± 0.09 mm thick band within seven days of incubation at a depth of 5-10 mm. *Methylocystis* sp. LW5 formed a band within four days at a depth of 14-19 mm and a thickness of 3.5 ± 0.12 mm. Together, these findings show the ability to identify reproducible differences between methanotrophic taxa cultured in this system.

A methane-oxygen counter gradient forms in the syringe model ecosystem

To determine if the syringe model ecosystem contained a methane-oxygen counter gradient, we measured the dissolved oxygen and methane content throughout LW13-inoculated and cell-free syringes after three days of incubation. In inoculated syringes, the dissolved oxygen concentration of the agarose closest to the filter tip was 336.9 ± 27.6 μmol/L and steeply declined to <1 μmol/L at the same depth as the horizontal band, around 25-30 mm from the filter tip (**Fig 1C**). Dissolved oxygen remained depleted with a mean concentration of 0.28 ± 0.09 μmol/L for the remainder of the agarose. This dissolved oxygen gradient began to form within 24 hours of flushing a methanotroph-inoculated gradient syringe and became steeper over the course of the three-day incubation period (**Fig S1**).

From the filter tip, the concentration of methane was <2 μmol/L until reaching the depth of the horizontal band, where it then increased in the remaining agarose up to 104.7 ± 42.67 μmol/L in the second-deepest agarose segment (**Fig 1C**). In cell-free sterile gradient syringes, a partial oxygen-methane counter gradient formed, but only reached a low of 270.6 ± 32.6 μmol/L dissolved oxygen and 5.79 ± 2.26 μmol/L methane in either gas gradient. These results indicate that bacterial consumption of methane and oxygen help drive the formation of the methane-oxygen counter gradient in this system, and that the intersection of the counter gradient is at the same location as the horizontal band.

Horizontal band formation is correlated with increased polysaccharide content but not increased viable cell counts

We initially hypothesized that the horizontal band contained a larger number of growing cells than the surrounding depths of the syringe. To test this, we counted the colony forming units (CFUs) per mL of agarose for inoculated syringes at different depths for each methanotroph strain (**Fig 2A**). Within one day after the appearance of a horizontal band, we extruded 1 mL agarose segments through a needle to count CFUs/mL. For all four methanotrophic strains tested, no individual segment contained a significantly higher CFUs/mL than any other segment from the same syringe, indicating that the formation of the horizontal band was not caused by increased viable cell numbers at that location.

Because methanotrophs are known to produce various polysaccharides under different growth conditions [20–22], we used a colorimetric assay [20, 23, 24] to quantify the relative polysaccharide content at different depths in the gradient syringe. After seven days of incubating LW13 with daily methane replenishment to increase the overall opacity and thickness of the band, we divided the agarose plug into 1 mL segments, ensuring the band was centered within a single segment.

In sterile gradient syringes, only the agarose matrix contributed to the colorimetric response of the assay, and thus the relative polysaccharide content at increasing depths remained constant (**Fig 2B**). In agarose segments inoculated with LW13, the segment containing the horizontal band had significantly increased (p <0.05) relative polysaccharide content compared to the other segments down to 33 mm in depth. The segment furthest from the filter tip trended upwards in relative polysaccharide content, which was consistent with the observation that a faint band occasionally formed at the interface of the agarose plug and the methane-filled headspace. Because these trends correlated to the observed band

position(s) within the gradient syringe, we conclude that the horizontal band formed as a result of increased polysaccharide production by cells positioned at the intersection of the methane-oxygen counter gradient.

Polysaccharide band formation within the gradient syringe is correlated to changes in gene expression

To investigate the cellular functions underlying the spatially resolved polysaccharide-producing phenotype observed in the gradient syringe, we compared transcriptomes of LW13 isolated from increasing depths in the agarose matrix. Late exponential/early stationary phase (**Fig S2**) gradient syringes inoculated with LW13 were divided into three 2 mL segments, with the middle segment centered around the polysaccharide band. These segments were designated "above", "band", and "below." Oxygen and methane profiles (**Fig 1C**) indicated differing gas substrate ratio for cells in these segments: high oxygen-low methane, low oxygen-low methane, and low oxygen-high methane, respectively. RNA-seq analysis of these segments revealed distinct gene expression profiles, with cells in the band and below segments exhibiting the greatest similarity (**Fig 3** and **S3**). Using a threshold of $|\log_2(\text{fold change})| > 1.5$ and adjusted $p < 0.0001$, we identified 11 differentially expressed genes (DEGs) between the band and the below segments, and 312 DEGs between the band and the above segments.

In the low oxygen micro-environment of the band segment, methane metabolism genes were generally downregulated compared to the higher oxygen above segment. The *pmoCAB* methane monooxygenase operon showed an average of 1.26 $\log_2$-fold decrease in band cells, while the *mxaF* and *xoxF* methanol dehydrogenase genes exhibited decreases of 0.623 and 1.02 $\log_2$-fold change, respectively. Accordingly, annotated ammonium uptake and denitrification genes were upregulated in the band segment. Using less stringent cutoffs, only one DEG was upregulated in the band segment compared to both above and below segments: a hypothetical protein within a predicted Type VI secretion system gene cluster. In comparing gene expression between band and below segments (**Fig S3A**), there were notably fewer DEGs with a $\log_2$-fold change >1.5 than in the band vs. above comparison, presumably due to the shared low oxygen micro-environments of the band and below segments. Among 11 upregulated DEGs were two genes predicted to be involved in iron acquisition and storage, and three genes predicted to be involved in cell division.

Comparing the gene expression between cells from the band segment and those from the above segment revealed a large range of DEGs with a $\log_2$-fold change >1.5, highlighting potential differences in cellular activity in these segments. In the band segment cells, there was significant upregulation of genes annotated as involved in energy production, amino acid and nucleotide metabolism/transport, coenzyme metabolism, and carbohydrate and lipid metabolism/transport compared to the above segment, as assigned by the NCBI Cluster of Orthologous Genes database [25]. These genes made up 78 of the 177 upregulated genes, suggesting involvement in diverse metabolic activities including energy conservation and synthesis of biomolecules. Additionally, 15 upregulated genes were predicted to be related to cellular structure and motility. Collectively, these upregulated genes suggest intensified activity in metabolism, biosynthesis, translation, transcription, cellular structure, and intracellular processes. Moreover, the increased expression of 17 genes predicted to be involved in intracellular trafficking and secretion, signal transduction, and secondary structure suggests enhanced intracellular communication and responsiveness to external conditions. Using less strict cutoffs, we found several putative functional pathways that were also upregulated, including electron transport, type VI secretion, hopanoid biosynthesis, and cell wall biosynthesis. These results reveal differences in gene expression within this spatially resolved model ecosystem.

Differentially expressed genes are involved in polysaccharide band formation

Among the upregulated genes with the greatest $\log_2$-fold change in the band compared to the above segment, we selected three for further investigation. We chose genes with annotated functions that to our knowledge had not been extensively studied in methanotrophs, especially in the context of polysaccharide production. These genes were predicted to encode a fucose 4-O-acetylase-like acetyltransferase (gene ID: 2923715777, Integrated Microbial Genomes System [26]**)**, a hemerythrin (2923717515), and an *N*-acyl amino acid synthase of PEP-CTERM/exosortase system (2923716464).

We constructed disruption mutant strains for each of the three genes to determine their individual influence on the growth of LW13 and the formation of the polysaccharide band within the gradient syringe (**Fig 3**). We disrupted the target genes via electroporation to create the mutant strains Δfucose, Δhemerythrin, and Δexosortase [27]. We then individually inoculated these LW13 mutants into gradient syringes, we observed the mutant strains did not form the same distinct polysaccharide band, but that band formation was restored after gene complementation (**Fig 4A**). We also counted the viable cells in each syringe after six days of incubation with daily methane replenishment to determine if these genes were involved in cell growth within the system. While wild-type LW13 grew to more than 75-times its initial CFU/mL concentration in the gradient syringe, the number of viable LW13Δfucose, LW13Δhemerythrin, and LW13Δexosortase mutant cells did not significantly (p <0.05) increase over the growth period (**Fig 4B**). Complementation of the deleted genes led to significantly increased growth in the three mutants from Day 0 to Day 6, restoring final CFU/mL to values comparable to the LW13 wild-type strain. Deletion of these genes did not negatively affect growth in planktonic culture, but instead led to slight but significantly faster growth rates (**Fig S4**). Together, these results show we can use the model gradient syringe system to link genes to phenotypes that would otherwise be missed using conventional culturing methods.

DISCUSSION

Methanotrophs use oxygen to catabolize methane as their sole carbon and energy source and often exist within a counter gradient of these gaseous substrates in the environment. In this work we observed that methanotrophs form a distinct horizontal band when grown in a spatially resolved model ecosystem containing a methane-oxygen counter gradient. We determined that the band is located at the intersection of the counter gradient and that it is not due to increased numbers of viable cells at this location, as previously hypothesized [16], but instead due to increased polysaccharide content at this location. We then used transcriptomics and deletion mutants to identify three genes involved in this phenotype. These genes are also required for cell growth within the model ecosystem, but their absence did not negatively affect the ability of LW13 to grow in planktonic culture.

The observed increase in polysaccharide content in the horizontal band in the gradient syringe model ecosystem may be due to increased extracellular polymeric substances (EPS) produced by methanotrophs at this depth. An established link exists between methane oxidation, oxygen availability, and EPS production in methylotrophic bacteria [20, 28]. However, more experiments will be necessary to determine the exact molecular components of this band, as well as whether they are within or outside of methanotrophic cells. Previously, the role of the exosortase protein EpsH in production of EPS in LW13 was identified [29] and confirmed [30], where disruption of *epsH* resulted in significantly reduced EPS in ammonium mineral salts media. However, this gene was not significantly differentially expressed by cells of any segment in our RNA-seq analysis (**Fig 3** and **S3**), possibly due to nitrate, rather than ammonium, being used as the nitrogen source in our experiments.

We observed variations in the depth and appearance of the horizontal band when we grew different methanotrophic genera in the gradient syringe (**Fig 1B**). This may stem from different methanotrophic genera being adapted to different oxygen tensions the environment [10, 11, 31]. It is unclear whether formation of the polysaccharide band is a cause or consequence of this location being at the intersection of the methane-oxygen counter gradient. It is possible that polysaccharide production is higher in cells at the intersection of the counter gradient as a response to low gas concentrations at this location, or that polysaccharide production led to higher gas consumption rates at this depth. While the exact triggers for polysaccharide production in methanotrophs remain to be precisely defined, excess carbon, nitrogen deficiency, and oxygen excess or limitation have all been reported to stimulate EPS production in methylotrophs [20, 21, 32]. Determining these factors may have practical implications for applied methanotrophy, such as methane mitigation in landfill covers and biofilters, which are negatively affected by the production of EPS [28].

Transcriptomic analysis of different segments within an LW13-inoculated gradient syringe revealed broad global gene expression differences, with band and below segments being most similar

(**Fig S3A**), suggesting that oxygen availability is a major influence on cellular heterogeneity. To explore possible gene-phenotype connections, we investigated a subset of genes that were upregulated in the band segment that had not yet been experimentally linked to polysaccharide production in methanotrophs. *N*-acyl amino acid synthases have been phylogenetically linked to the PEP-CTERM/exosortase system [33], a putative protein sorting system in Gram-negative bacteria associated with EPS production [34]. The predicted product of the fucose 4-O-acetylase like acetyltransferase gene likely engages in acylation processes impacting various sugar-containing cell-surface structures, including exopolysaccharides [35]. Hemerythrin is a non-heme oxygen-binding protein that serves as an oxygen scavenging transporter for pMMO-containing aerobic methanotrophs such as LW13 [31]. Single knockouts of these genes in LW13 had a negative effect on horizontal band formation (**Fig 4A**) and growth (**Fig 4A**) in the gradient syringe model ecosystem, but did not interfere with growth in planktonic culture (**Fig S4**). The fact that band formation and growth were both affected in each of the mutants means that it is possible that methanotrophic growth is dependent on horizontal band formation in this system, or that formation of the band is dependent on growth.

In this work we demonstrate that culturing methanotrophs within a spatially resolved counter gradient of methane and oxygen can reveal gene-phenotype associations that are largely unnoticed in conventional culturing approaches. Our results have raised questions about methanotroph physiology within a methane-oxygen counter gradient that can now be studied at the molecular level using this model ecosystem in the future. More broadly, this study highlights the utility of even simple laboratory-based model ecosystems for linking genes with organismal phenotypes.

ACKNOWLEDGEMENTS

This work was supported by startup funding from the University of Utah Department of Chemistry. We thank members of the Puri Lab for helpful discussions.

AUTHOR CONTRIBUTIONS

D.G.B. and A.W.P. designed the experiments, analyzed the data, and wrote the manuscript. D.G.B. performed the experiments. D.G.B. and A.W.P. edited and approved of the final version of the manuscript.

CONFLICTS OF INTEREST

The authors declare no conflicts of interest.

METHODS

Strain growth

Liquid cultures of *Methylomonas* sp. LW13 were grown in an atmosphere of 50% methane in air in liquid nitrate mineral salts (NMS) medium containing 0.2 g/liter $MgSO_4 \cdot 7H_2O$, 0.2 g/liter $CaCl_2 \cdot 6H_2O$, 1 g/liter KNO_3, and 30 µM $LaCl_3$ as well as 1X trace elements; 500X trace elements contain 1.0 g/liter Na_2-EDTA, 2.0 g/liter $FeSO_4 \cdot 7H_2O$, 0.8 g/liter $ZnSO_4 \cdot 7H_2O$, 0.03 g/liter $MnCl_2 \cdot 4H_2O$, 0.03 g/liter H_3BO3, 0.2 g/liter $CoCl_2 \cdot 6H_2O$, 0.6 g/liter $CuCl_2 \cdot 2H_2O$, 0.02 g/liter $NiCl_2 \cdot 6H_2O$, and 0.05 g/liter $Na_2MoO \cdot 2H_2O$. A final concentration of 5.8 mM phosphate buffer (pH 6.8) was added before use. Liquid cultures were grown in 18 x 150 mm tubes sealed with rubber stoppers and aluminum seals, and were shaken at 200 rpm at room temperature.

Preparation of gradient syringes

Liquid cultures of methanotrophs in exponential-phase growth (OD_{600} ~ 0.5) were used to inoculate gradient syringes. Cells were pelleted and resuspended in sterile water to reach an approximate OD_{600} of 1.0. For each 10 mL syringe, 1 mL of concentrated cells was mixed with 5 mL NMS1 and 4 mL molten agarose (0.5% w/v, cooled to 55°C). The mixture was slowly poured to the 8 mL marking of a 10 mL plastic Luer-Lok tip syringe (BD) fitted with a sterile PTFE filter tip (Titan3 PTFE (Hydrophobic) Syringe Filter 0.2 µm, 4 mm, Thermo Scientific). Solidified syringes were capped with a sterile 20 mm rubber butyl stopper (Chemglass Life Sciences) and wrapped with lab tape for labeling. Inlet and outlet needles (23 gauge, BD) were pierced through the rubber stopper, and 20 mL of 100% CH_4 was flushed through the syringe headspace. Syringes were flushed daily with methane and incubated with the PTFE filter pointing up at 18°C.

Gas analysis of gradient syringes

The dissolved oxygen within the gradient syringe was measured using a Clark-type microelectrode (Ox50, Unisense) at 0.1 mm intervals. Immediately before measurement, the tip of a syringe was sliced off with a razor and the syringe fastened to a syringe pump (NE-1000, New Era Pump Systems Inc.) that moved the agarose plug towards the microelectrode at a rate of 1 mL per minute (0.6 cm/min). Measurements were recorded and converted to µmol/L using the Unisense Logger software. The relative methane concentration in LW13-containing and cell-free gradient syringe agarose were analyzed using gas chromatograph-flame ionization detector. Just before extrusion, the syringe filter was replaced with a two-way stopcock with a 23-gauge needle and the syringe's rubber stopper was quickly exchanged with a syringe plunger. Eight 1 mL agarose aliquots were then added to different evacuated 12 mL Exetainer vials (Labco). Prior to injecting 500 µL of headspace into an Agilent 6890N gas chromatograph, sample vials were equilibrated to atmospheric pressure. A calibration curve employing known CH_4 amounts in vials was used to convert peak area (pA*min) to µmol/L.

Counting of viable methanotroph cells in gradient syringe

Inoculated agarose within the gradient syringe was extruded in 1 mL aliquots through a 23-gauge sterile needle using the accompanying syringe plunger. Agarose was diluted with 1 mL sterile water and vortexed homogenize the samples and aid in pipetting. Samples were serially diluted tenfold in sterile water before spotting onto solid NMS agar plates. Plates were incubated in sealed jars under 40% methane in air and grown at 18°C. Bacterial colonies were counted and used to calculate the colony forming units per milliliter (CFUs/mL).

Polysaccharide detection assay

One milliliter aliquots of agarose were extruded into 2 mL microcentrifuge tubes and mixed with 1 mL of a 1% (m/v) Na_2CO_3 solution in water. Samples were heated to 80°C for 30 minutes and vortexed every 5-10 minutes, followed by centrifugation at 4,000 x g at 4°C for 20 minutes. The supernatant was collected and combined with three volumes of 100% ethanol and incubated at -20°C overnight. The ethanol-precipitated polysaccharides were collected by centrifugation at 16,100 x g at 4°C for 30 minutes, and the air-dried pellet was resuspended in 100 uL of Milli-Q water. The relative polysaccharide content of

336 each agarose segment was measured using a phenol-sulfuric acid colorimetric assay. Briefly, 50 µL of
337 resuspended extract was combined with 150 µL concentrated sulfuric acid and 30 uL of 5% phenol in a
338 clear 96-well plate [20, 23, 24]. The absorbance at 490 nm was measured using a microplate reader, and
339 the relative polysaccharide content of individual agarose segments was calculated as a percentage of
340 the absorbance at the agarose segment closest to the PTFE filter.
341
342 **RNA preparation, RNA-seq, and data analysis**
343 For each of three independent replicates, eight *Methylomonas* sp. LW13-inoculated syringes were
344 incubated for three days to reach exponential growth. Agarose segments (2 mL) positioned above, at,
345 and below the polysaccharide band were extruded from each syringe through a 23-gauge needle into
346 microcentrifuge tubes. Samples were frozen at -80°C until RNA extraction. Thawed aliquots were
347 centrifuged at 21,000 x g at 4°C for 15 minutes. After removal of the supernatant, 600 µL of pre-warmed
348 CTAB extraction buffer was added. The CTAB buffer consisted of 2% CTAB, 2% polyvinylpyrrolidone 40,
349 2 M sodium chloride, 100 mM Tris-HCl (pH 8.0), and 20 mM EDTA [36]. Zirconia glass beads were added,
350 and samples were homogenized for 3 minutes at 30 Hz/sec using a bead beater. Samples were extracted
351 twice with 600 µL chloroform:isoamyl alcohol (24:1), and the aqueous phase was mixed with isopropanol
352 and incubated overnight at -20°C. Precipitates were centrifuged for 30 minutes at 16,100 x g at 4°C for
353 30 minutes and pellets were washed twice with cold 75% ethanol made with DEPC water. Air dried pellets
354 were dissolved in 100 uL DEPC water and treated with DNase I (Ambion) at 37°C for 30 minutes. The
355 DNase I was inactivated by extraction with three volumes of acid phenol:chloroform:IAA (125:24:1, pH
356 4.5) before pooling RNA from the same segment across all syringes in an overnight precipitation at -20°C
357 in 1 volume isopropanol and 0.8 M LiCl. Precipitates were washed twice with cold 70% ethanol made
358 with DEPC water, air dried, and resuspended in 50 uL DEPC water. Samples were re-purified using RNA
359 Clean & Concentrator-5 (Zymo Research) to remove small RNAs.
360 Library preparation and sequencing were performed by the High-Throughput Genomics Shared
361 Resource Core at the University of Utah. cDNA libraries were prepared using a NEBNext Ultra II
362 Directional RNA Library Prep Kit with rRNA Depletion (New England Biolabs) and sequenced using an
363 Illumina NovaSeq 6000 with 150x150 cycle paired end sequence run. RNA sequencing data analysis
364 was conducted using a KBASE workflow [37]. Reads quality was assessed using FastQC v0.11.9,
365 trimmed with Trimmomatic v0.36 [38], aligned using HISAT2 v2.1.0 [39], transcripts assembled with
366 StringTie v2.1.5 [40], and differentially expressed genes identified using DESeq2 v1.20.0 [41].
367
368 **Genetic manipulation in *Methylomonas* sp. LW13**
369 Plasmids and constructs used in this study are listed in **Table S1**, and primers are listed in **Table S2**. All
370 genetic manipulation of LW13 was carried out at 30°C under 50% methane in air.
371 *Deletion mutant construction:* Genetic manipulations were accomplished by electroporating PCR
372 amplification-generated constructs into LW13, followed by the selection of chromosomal recombinants,
373 following established methods [27]. Briefly, the kanamycin resistance gene cassette (amplified from
374 plasmid pCM433kanT [42]) and flanking regions of the target gene were assembled using overlap
375 extension PCR. The assembled fragment was then amplified using nested primers and purified by gel
376 purification. After confirming correct assembly via Sanger sequencing the fragment was electroporated
377 directly into LW13 cells. Post-electroporation, cells were cultured overnight in NMS1 medium without
378 antibiotics, and then transferred to kanamycin-containing plates (50 µg/ml). Single colonies were
379 selected, and disruption of the gene of interest with the kanamycin resistance cassette was confirmed
380 through colony PCR using OneTaq with primers specific to the assembled construct.
381 *Complementation of genes into mutant strains:* Using overlap extension PCR, ~3000-nucleotide
382 sequences containing the gene of interest were constructed and electroporated into LW13 mutants.
383 These constructs included the gene of interest under the bacterial promoter *nptII* [43], along with a zeocin
384 resistance gene cassette directly downstream of the gene to be complemented. Flanking either end of
385 this construct were homologous flanks targeting an insertion site in the LW13 genome that was previously
386 used for complementation in this strain [44]. Full-length DNA segments were excised after separation on
387 a 1% TAE agarose gel and purified using a ThermoFisher GeneJet Gel Purification Kit. After introduction

388 of the segments via electroporation, successful recombinants were selected on NMS1 media containing
389 20 µg/mL zeocin and confirmed by colony PCR.
390
391 **Accession number(s).** Raw transcriptomic data, as well as normalized counts and computed pairwise
392 fold changes for the different syringe segments have been submitted to the NIH NCBI Gene Expression
393 Omnibus (GEO) database under accession number GSE243827.

REFERENCES

1. Zhalnina K, Zengler K, Newman D, Northen TR. Need for Laboratory Ecosystems To Unravel the Structures and Functions of Soil Microbial Communities Mediated by Chemistry. *mBio* 2018; **9**: e01175-18.
2. Zengler K, Hofmockel K, Baliga NS, Behie SW, Bernstein HC, Brown JB, Dinneny JR, Floge SA, Forry SP, Hess M, Jackson SA, Jansson C, Lindemann ST, Pett-Ridge J, Maranas C, Venturelli OS, Wallenstein MD, Shank EA, Northen TR. EcoFABs: advancing microbiome science through standardized fabricated ecosystems. *Nat Methods* 2019; **16**: 567–571.
3. Chistoserdova L, Kalyuzhnaya MG, Lidstrom ME. The Expanding World of Methylotrophic Metabolism. *Annu Rev Microbiol* 2009; **63**: 477–499.
4. Stein LY, Klotz MG. The nitrogen cycle. *Curr Biol* 2016; **26**: R94–R98.
5. Semrau JD. Bioremediation via Methanotrophy: Overview of Recent Findings and Suggestions for Future Research. *Front Microbiol* 2011; **2**.
6. Reim A, Lüke C, Krause S, Pratscher J, Frenzel P. One millimetre makes the difference: high-resolution analysis of methane-oxidizing bacteria and their specific activity at the oxic-anoxic interface in a flooded paddy soil. *ISME J* 2012; **6**: 2128–2139.
7. Auman AJ, Stolyar S, Costello AM, Lidstrom ME. Molecular Characterization of Methanotrophic Isolates from Freshwater Lake Sediment. *Appl Environ Microbiol* 2000; **66**: 5259–5266.
8. Smith GJ, Angle JC, Solden LM, Borton MA, Morin TH, Daly RA, Johnston MD, Stefanik KC, Wolfe R, Gil B, Wrighton KC. Members of the Genus *Methylobacter* Are Inferred To Account for the Majority of Aerobic Methane Oxidation in Oxic Soils from a Freshwater Wetland. *mBio* 2018; **9**: e00815-18.
9. Brune A, Frenzel P, Cypionka H. Life at the oxic–anoxic interface: microbial activities and adaptations. *FEMS Microbiol Rev* 2000; **24**: 691–710.
10. Oshkin IY, Beck DA, Lamb AE, Tchesnokova V, Benuska G, McTaggart TL, Kalyuzhnaya MG, Dedysh SN, Lidstrom ME, Chistoserdova L. Methane-fed microbial microcosms show differential community dynamics and pinpoint taxa involved in communal response. *ISME J* 2015; **9**: 1119-1129.
11. Hernandez ME, Beck DAC, Lidstrom ME, Chistoserdova L. Oxygen availability is a major factor in determining the composition of microbial communities involved in methane oxidation. *PeerJ* 2015; **3**: e801.
12. Strong PJ, Xie S, Clarke WP. Methane as a Resource: Can the Methanotrophs Add Value? *Environ Sci Technol* 2015; **49**: 4001–4018.
13. Davidson EA, Semrau JD, Nguyen NK. Improved scientific knowledge of methanogenesis and methanotrophy needed to slow climate change during the next 30 years. *mBio* 2023; e02059-23.
14. Murase J, Frenzel P. A methane-driven microbial food web in a wetland rice soil. *Environ Microbiol* 2007; **9**: 3025–3034.
15. Sinke AJC, Cottaar FHM, Buis K, Keizer P. Methane Oxidation by Methanotrophs and Its Effects on the Phosphate Flux over the Sediment-Water Interface in a Eutrophic Lake. *Microb Ecol* 1992; **24**: 259–269.
16. Bussmann I, Rahalkar M, Schink B. Cultivation of methanotrophic bacteria in opposing gradients of methane and oxygen. *FEMS Microbiol Ecol* 2006; **56**: 331–344.
17. Amaral JA, Knowles R. Growth of methanotrophs in methane and oxygen counter gradients. *FEMS Microbiol Lett* 1995; **126**: 215–220.
18. Danilova OV, Suzina NE, Van De Kamp J, Svenning MM, Bodrossy L, Dedysh SN. A new cell morphotype among methane oxidizers: a spiral-shaped obligately microaerophilic methanotroph from northern low-oxygen environments. *ISME J* 2016; **10**: 2734–2743.
19. Kalyuzhnaya MG, Lamb AE, McTaggart TL, Oshkin IY, Shapiro N, Woyke T, Chistoserdova L. Draft Genome Sequences of Gammaproteobacterial Methanotrophs Isolated from Lake Washington Sediment. *Genome Announc* 2015; **3**: e00103-15.
20. Chiemchaisri W, Wu JS, Visvanathan C. Methanotrophic production of extracellular polysaccharide in landfill cover soils. *Water Sci Technol* 2001; **43**: 151–159.

21. Khmelenina VN, Kalyuzhnaya MG, Sakharovsky VG, Suzina NE, Trotsenko YA, Gottschalk G. Osmoadaptation in halophilic and alkaliphilic methanotrophs. *Arch Microbiol* 1999; **172**: 321–329.
22. Gilman A, Laurens LM, Puri AW, Chu F, Pienkos PT, Lidstrom ME. Bioreactor performance parameters for an industrially-promising methanotroph *Methylomicrobium buryatense* 5GB1. *Microb Cell Fact* 2015; **14**: 1–8.
23. Masuko T, Minami A, Iwasaki N, Majima T, Nishimura S-I, Lee YC. Carbohydrate analysis by a phenol–sulfuric acid method in microplate format. *Anal Biochem* 2005; **339**: 69–72.
24. Felz S, Al-Zuhairy S, Aarstad OA, van Loosdrecht MCM, Lin YM. Extraction of Structural Extracellular Polymeric Substances from Aerobic Granular Sludge. *J Vis Exp* 2016; e54534.
25. Galperin MY, Makarova KS, Wolf YI, Koonin EV. Expanded microbial genome coverage and improved protein family annotation in the COG database. *Nucleic Acids Res* 2015; 43: D261–D269.
26. Chen I-MA, Chu K, Palaniappan K, Ratner A, Huang J, Huntemann M, Hajek P, Ritter SJ, Webb C, Wu D, Varghese NJ, Reddy TBK, Mukherjee S, Ovchinnikova G, Nolan M, Seshadri R, Roux S, Visel A, Woyke T, Eloe-Fadrosh EA, Kyrpides NC, Ivanova NN. The IMG/M data management and analysis system v.7: content updates and new features. *Nucleic Acids Res* 2023; **51**: D723–D732.
27. Yan X, Chu F, Puri AW, Fu Y, Lidstrom ME. Electroporation-based genetic manipulation in type I methanotrophs. *Appl Environ Microbiol* 2016; **82**: 2062–2069.
28. He R, Ma R-C, Yao X-Z, Wei X-M. Response of methanotrophic activity to extracellular polymeric substance production and its influencing factors. *Waste Manag* 2017; **69**: 289–297.
29. Zheng Y, Huang J, Zhao F, Chistoserdova L. Physiological Effect of XoxG(4) on Lanthanide-Dependent Methanotrophy. *mBio* 2018; **9**: e02430-17.
30. Wang H, Zheng Y, Zhu B, Zhao F. *In situ* role of extracellular polymeric substances in microbial electron transfer by *Methylomonas* sp. LW13. *Fundam Res* 2021; **1**: 735–741.
31. Guerrero-Cruz S, Vaksmaa A, Horn MA, Niemann H, Pijuan M, Ho A. Methanotrophs: Discoveries, Environmental Relevance, and a Perspective on Current and Future Applications. *Front Microbiol* 2021; **12**: 678057.
32. Linton JD, Watts PD, Austin RM, Haugh DE, Niekus HGD. The Energetics and Kinetics of Extracellular Polysaccharide Production From Methanol by Micro-organisms Possessing Different Pathways of C1 Assimilation. *J Gen Microbiol* 1986; **132**: 779–788.
33. Craig JW, Cherry MA, Brady SF. Long-Chain *N*-Acyl Amino Acid Synthases Are Linked to the Putative PEP-CTERM/Exosortase Protein-Sorting System in Gram-Negative Bacteria. *J Bacteriol* 2011; **193**: 5707–5715.
34. Haft DH, Paulsen IT, Ward N, Selengut JD. Exopolysaccharide-associated protein sorting in environmental organisms: the PEP-CTERM/EpsH system. Application of a novel phylogenetic profiling heuristic. *BMC Biol* 2006; **4**: 29.
35. Pearson C, Tindall S, Potts JR, Thomas GH, van der Woude MW. Diverse functions for acyltransferase-3 proteins in the modification of bacterial cell surfaces. *Microbiology* 2022; **168**.
36. Wang L, Stegemann JP. Extraction of High Quality RNA from Polysaccharide Matrices using Cetlytrimethylammonium Bromide. *Biomaterials* 2010; **31**: 1612.
37. Arkin AP, Cottingham RW, Henry CS, Harris NL, Stevens RL, Maslov S, *et al.* KBase: The United States Department of Energy Systems Biology Knowledgebase. *Nat Biotechnol* 2018; **36**: 566–569.
38. Bolger AM, Lohse M, Usadel B. Trimmomatic: a flexible trimmer for Illumina sequence data. *Bioinformatics* 2014; **30**: 2114–2120.
39. Kim D, Paggi JM, Park C, Bennett C, Salzberg SL. Graph-based genome alignment and genotyping with HISAT2 and HISAT-genotype. *Nat Biotechnol* 2019; **37**: 907–915.
40. Pertea M, Pertea GM, Antonescu CM, Chang T-C, Mendell JT, Salzberg SL. StringTie enables improved reconstruction of a transcriptome from RNA-seq reads. *Nat Biotechnol* 2015; **33**: 290–295.
41. Love MI, Huber W, Anders S. Moderated estimation of fold change and dispersion for RNA-seq data with DESeq2. *Genome Biol* 2014; **15**: 550.
42. Puri AW, Owen S, Chu F, Chavkin T, Beck DAC, Kalyuzhnaya MG, Lidstrom ME. Genetic tools for the industrially promising methanotroph *Methylomicrobium buryatense*. *Appl Environ Microbiol* 2015; **81**: 1775–1781.

43. Yenofsky RL, Fine M, Pellow JW. A mutant neomycin phosphotransferase II gene reduces the resistance of transformants to antibiotic selection pressure. *Proc Natl Acad Sci* 1990; **87**: 3435–3439.
44. Puri AW, Liu D, Schaefer AL, Yu Z, Pesesky MW, Greenberg EP, Lidstrom ME. Interspecies Chemical Signaling in a Methane-Oxidizing Bacterial Community. *Appl Environ Microbiol* 2019; **85**: e02702-18.

FIGURES

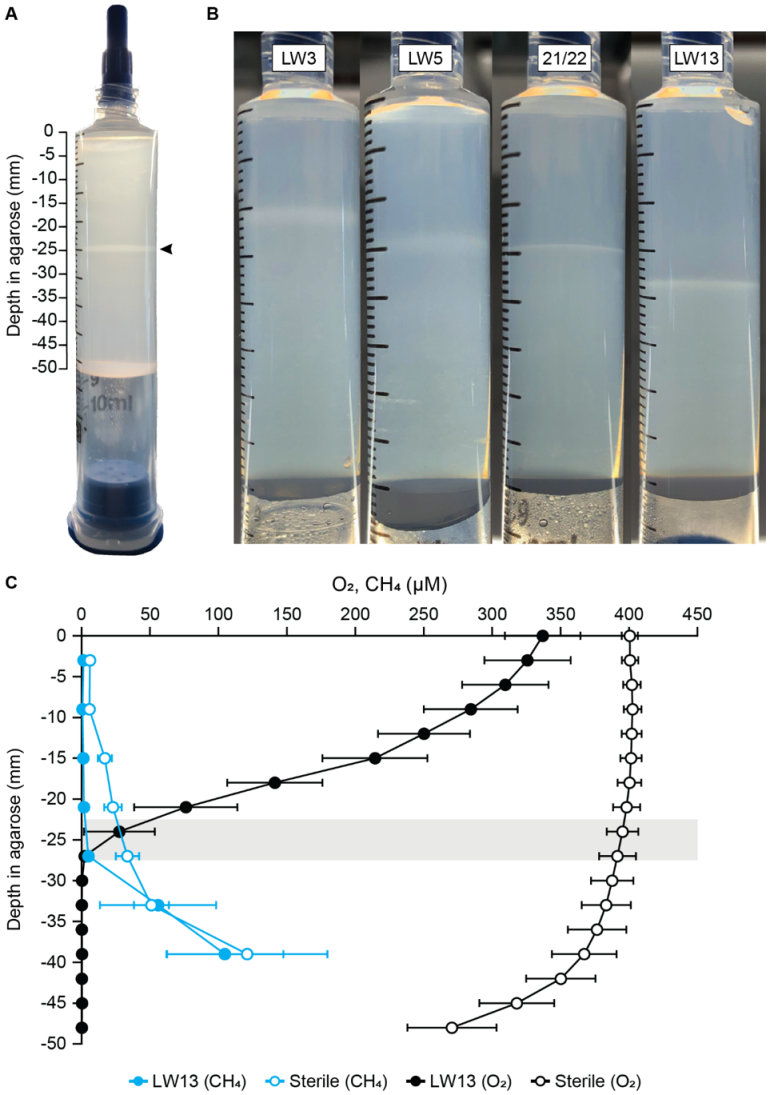

FIGURE 1. (**A**) The gradient syringe model ecosystem inoculated with the methanotroph *Methylomonas* sp. strain LW13. Black arrowhead indicates location of the horizontal band. (**B**) Cultivation of the Lake Washington-isolated methanotrophic strains in the gradient syringe, *Methylosinus* sp. strain LW3 (day 7 within the syringe), *Methylobacter tundripaludum* 21/22 (day 7), *Methylocystis* sp. strain LW5 (day 7), *Methylomonas* sp. strain LW13 (day 3). Images are representative of three independent experiments. (**C**) Methane (blue) and oxygen (black) gradients of inoculated (solid) and sterile (open) syringes after three days of incubation. Both substrates are depleted at the same depth as the horizontal band (gray bar) that forms within 25-30 mm from the filter tip.

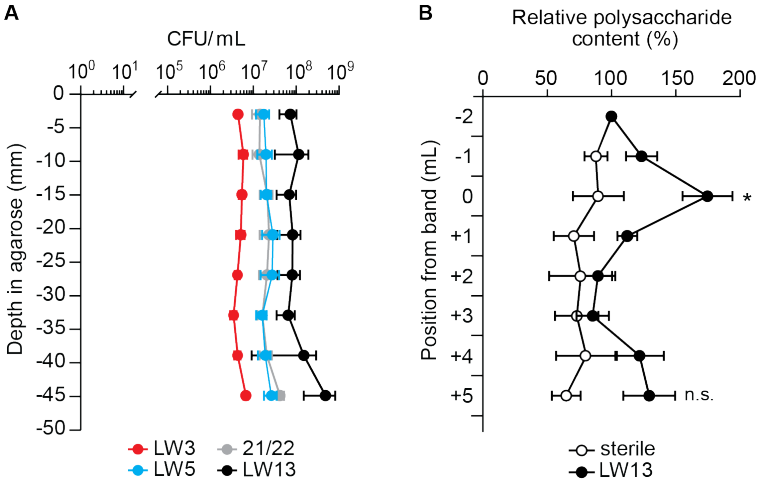

FIGURE 2. (**A**) Distribution of viable methanotrophic cells in the gradient syringe model ecosystem. The mean CFU/mL from any segment of any strain is not significantly different than any other segment mean CFU/mL of the same strain; one-way ANOVA (p <0.05). (**B**) Relative polysaccharide content from 1 mL agarose segments, with 0 representing a 1 mL segment centered around the horizontal band. Individual absorbance values for each syringe replicate are reported as a percentage of the absorbance at 490 nm measured at the segment closest to the filter tip from the same syringe. Data show the mean ± standard deviation of three independent experiments with two technical replicates each. *, significantly different from all other LW13 segment datapoints except the +5 point denoted n.s. (not significant); two-tailed heteroscedastic t test (p <0.05).

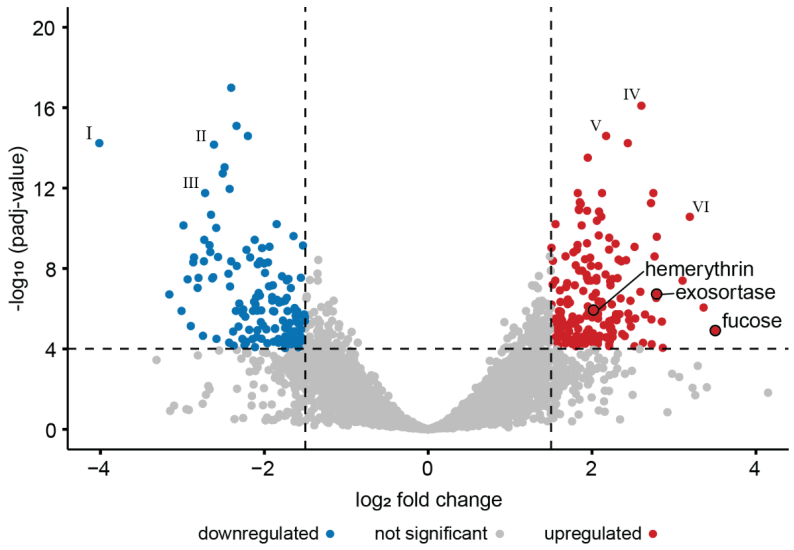

FIGURE 3. Differentially expressed genes in the band segment compared to the above segment. Dashed vertical lines signify cutoffs of |$\log_2$-fold change| >1.5 and the horizontal line indicates a cutoff of *p* value <0.0001. Predicted functions of highlighted genes: (I) transposase-like protein, (II) heme oxygenase, (III) polyhydroxybutyrate depolymerase, (IV) tryptophan synthase alpha chain, (V) acetyl-CoA carboxylase carboxyl transferase subunit beta, (VI) ornithine carbamoyltransferase.

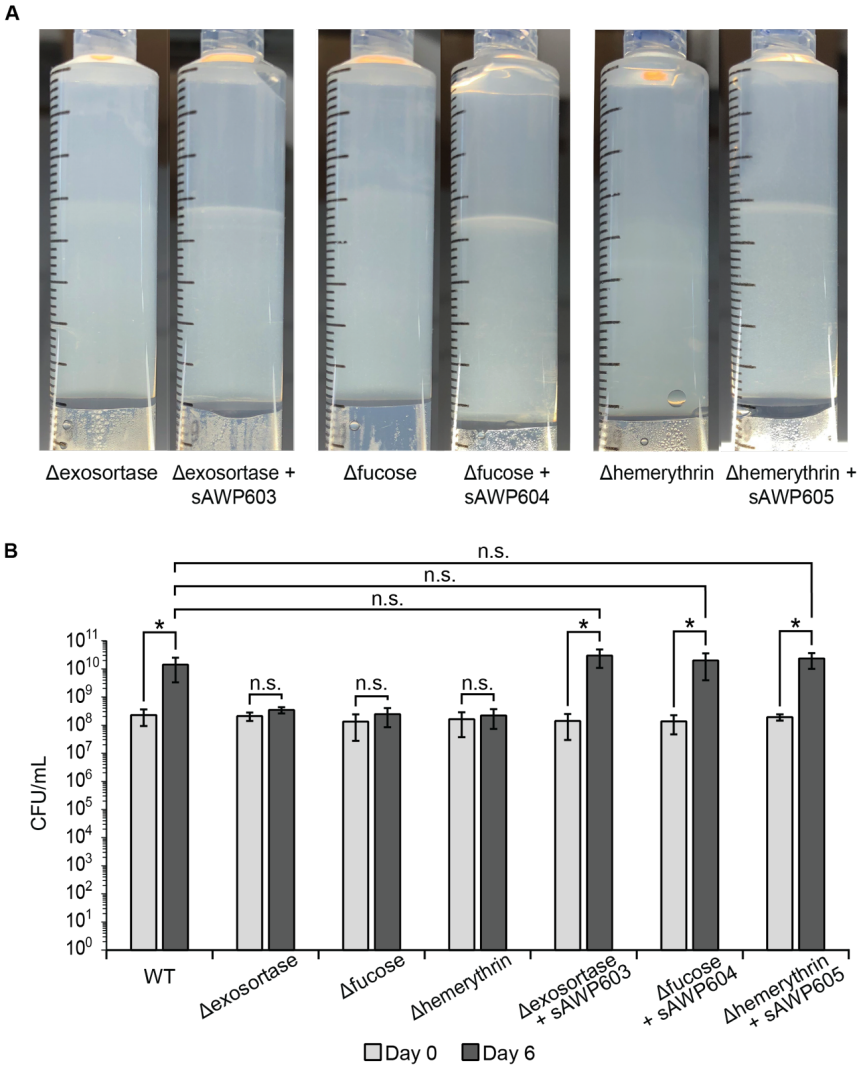

FIGURE 4. (**A**) Reduction in polysaccharide band production in three LW13 mutants within the gradient syringe. Images are representative of three independent experiments. (**B**) Growth of LW13 strains in the gradient syringe over a six-day incubation period. Data show the mean ± standard deviation of three independent experiments with two technical replicates each. *, significantly different (two-tailed heteroscedastic *t* test, α = 0.05). n.s., not significantly different.